Long-lived isomeric states and quasiparticle band structures in neutron-rich ^{162,164}Gd nuclei from β decay

E. H. Wang[1], J. M. Eldridge,[1] N. T. Brewer,[2] J. H. Hamilton,[1] J. C. Batchelder,[3] Y. X. Liu,[4] Y. Sun,[5] C. Brown,[1]
C. J. Zachary,[1] B. M. Musangu,[1] A. V. Ramayya,[1] K. P. Rykaczewski,[2] C. J. Gross,[2] R. Grzywacz,[2,6] M. Madurga,[6] D. Miller,[6]
D. W. Stracener,[2] C. Jost,[6] E. F. Zganjar,[7] J. A. Winger,[8] M. Karny,[9] S. V. Paulauskas,[6] S. H. Liu,[2] M. Wolińska-Cichocka,[2,10]
S. W. Padgett,[6] A. J. Mendez II,[11] K. Miernik,[2,9] A. Fijałkowska,[9] and S. V. Ilyushkin[8]

[1]*Department of Physics and Astronomy, Vanderbilt University, Nashville, Tennessee 37235, USA*
[2]*Physics Division, Oak Ridge National Laboratory, Oak Ridge, Tennessee 37830, USA*
[3]*Nuclear Engineering Department, University of California Berkeley, California 94720, USA*
[4]*Department of Physics, Huzhou University, Huzhou 313000, People's Republic of China*
[5]*School of Physics and Astronomy, Shanghai Jiao Tong University, Shanghai 200240, People's Republic of China*
[6]*Department of Physics and Astronomy, University of Tennessee, Knoxville, Tennessee 37996, USA*
[7]*Department of Physics and Astronomy, Louisiana State University, Baton Rouge, Louisiana 70803, USA*
[8]*Department of Physics and Astronomy, Mississippi State University, Mississippi 39762, USA*
[9]*Faculty of Physics, University of Warsaw, Warsaw PL-02-093, Poland*
[10]*Heavy Ion Laboratory, University of Warsaw, Warsaw PL 02-093, Poland*
[11]*Campbell University, Buies Creek, North Carolina 27506, USA*

Neutron-rich nuclei ^{162,164}Eu were produced by bombarding a proton beam on a ^{238}U target at the Holifield Radioactive Ion Beam Facility at Oak Ridge National Laboratory and mass separating the ^{162,164}Eu products. New level schemes and new γ-ray transitions of the daughters ^{162,164}Gd were identified from β-decay spectroscopy studies. Half-lives of the ^{162,164}Eu were remeasured to clarify the previous ambiguous results. Two quasiparticle band structures were built and compared with neighboring nuclei. The β and γ bands were extended in ^{162}Gd and a γ band was extended in ^{164}Gd. Half-lives of the isomeric states at (6^-) 1449 keV in ^{162}Gd and (4^-) 1096 keV in ^{164}Gd were measured to be 99(3) μs and 0.56(3) μs, respectively. Projected shell model calculations were performed and found to be in good agreement with all of the experimental data.

I. INTRODUCTION

Neutron-rich nuclei in the $A \sim 160$ region have drawn much attention in nuclear physics studies. In this region, nuclei with neutron number $N \geqslant 94$ become strongly deformed with large quadrupole deformations. Maximum abundance in the r-process is seen in this rare-earth region [1], and arises from this large deformation at midshell [2]. Nuclear structure studies in this region are important to understand the competion between neutron capture and β decay in r-process stellar nucleosynthesis. From experiment, limited stucture information was known compared to other regions due to difficulties to populate the neutron-rich isotopes. Previous experimental studies show energies of the 2^+ levels have a local minimum at $N = 98$ [3,4]. This fact is in contrast with the theoretical calculations for deformation maximum at $N = 104$ midshell [5]. Recently, two quasiparticle bands and isomers have been reported in ^{154,156,158,160}Nd [6,7], ^{156,158,160,162,164}Sm [6,8–12], ^{162,164,166}Gd [9,12–14] by ^{238}U, ^{239}Pu induced fission and ^{252}Cf spontaneous fission.

Specifically, in the previous study of ^{162,164}Gd, ^{162}Gd excited levels up to ≈ 2.5 MeV were reported in the ^{160}Gd(t, p) ^{162}Gd reaction [15], with several positive parity levels assigned. Later, our group extended the ground state band up to 16^+ [3]. Recently, β-decay experiments observed a 6^- state and the 5^+, 6^+ member of the 1γ-vibrational band of this nucleus [13]. For ^{164}Gd, our previous work established the ground state band up to 14^+ [3]. Osa *et al.* [16] observed three γ rays but did not place them in the level scheme. Additionally, several new works [9,11,14] based on isomeric decay from a 4^- state added two new non-yrast levels and three new γ rays to the level scheme of ^{164}Gd. In the present work, we have confirmed and extended the previous reported 1γ-vibrational band levels and extended the band structure built on the isomeric states in ^{162,164}Gd. New spin and parity assignments have been made for the Eu parents according to our present work. Projected shell model calculations have been performed and compare favorably with the experimental data.

II. EXPERIMENTAL SETUP

The current experiment was performed at the Holifield Radioactive Ion Beam Facility (HRIBF) at Oak Ridge

Mass number	Eu half-life	Gd half-life	Beam on/off
162	10.6(10) s [17]	8.2(3) min [18], 8.55(28) min [19]	22 s/22 s
164	4.2(2) s [16]	45(3) s [20]	8 s/8 s

Naitonal Laboratory. A 10–18 μA $\approx$ 50 MeV proton beam was used to bombard the UCx target on a High-Voltage (HV) platform. The induced fission fragments as positive ions at 40 keV were seleted by passing through a dipole magnet with resolution of $m/\Delta m \sim 1000$. These ions were then accelerated to 200 keV and Eu was separated by a second magnet with $m/\Delta m \sim 10000$ resolution. A fast beam deflector (kicker) was used to prevent the beam from reaching the detection station. This kicker was operated in a correlated way with a tape cycle, as discussed below. The ion beam was implanted into a movable tape at the turning point of the moving tape collector (MTC) inside the Low-energy Radioactive Ion Beam Spectroscopy Station (LeRIBSS). This point was surrounded by four high-purity germanium (HPGe) detectors and two plastic scintillators in a co-axial arragement for β detection. In the beam accumulation period, the kicker was turned on and the ion beam was transmitted to the MTC. In the decay period, the kicker was turned off to deflect the beam away. After the decay period, the MTC moved $\approx$50 cm away within about 400 ms to a shielded place. The beam on/off settings of the tape cycle are listed in Table. I. The β detectors provided β-gated events. The acquisition system was operated in a triggerless mode and was time stamped with a 10 ns pulse from a clock. This acquisition allows for variable coincidence gates. Details of the experimental setup can be found in Refs. [21,22]. Here $A = 81, 82$ nuclei are the major contaminants (not from fission of Eu) because their atomic numbers are half of those the current ^{162,164}Eu ones and have similar m/Q and were selected by the magnet. The ^{162,164}Eu were in the 2^+ charge state while the contaminant $A = 81, 82$ in the beam were at 1^+, so both of them are selected by the magnet. The β-decay and β-n decay daughters of the $A = 81, 82$ nuclei are also present but weaker.

III. EXPERIMENTAL RESULTS

A. ^{162}Gd

The new level scheme of ^{162}Gd is shown in Fig. 1. The γ-ray transition intensities are measured and listed in Table II. The energy levels are grouped into six bands. The ground state (g.s.) band was established up to 16^+ in Ref. [3] from ^{252}Cf spontaneous fission. In the present work, the g.s. band is confirmed up to 8^+. In Ref. [15], 864 keV 2^+, 930 keV 3^+, and 1015 keV 4^+ were assigned as the γ-vibrational band levels without linking transitions and were reported to have about 7-keV uncertainty. In the present study, these levels are confirmed more accurately as 863.0, 927.4, and 1012.7 keV, respectively, by identifying the linking transitions from the γ-vibrational band to the g.s. band. The 630-, 755-, 884-, 1010-keV transitions from the γ-vibrational band to the g.s.

band were reported previously from the ^{162}Eu β decay [13]. In the present work, they are identified as 628.4, 753.7, 881.9, and 1007.1 keV, respectively. The current work also identified the 7^+ state of the γ-vibrational band as shown in the level scheme in Fig. 1. In Ref. [23], the 863.3- and 792.0-keV transitions depopulating the 863.3-keV 2^+ γ band level, as well as the strong 856.5-keV transition depopulating the 927.9-keV 3^+ γ band level were reported. Those transitions and levels are confirmed in the present work. The odd and even spin levels of the γ band are separated to make them easy to be seen in the figure since their energies are too close. The 12 levels located on the left of the level scheme are assumed as non-band levels. The decay patterns of those levels indicate different spin ranges. The 2305-, 2414-, 2418-, and 3573-keV levels only decay to the 71.7-keV 2^+ state. They are proposed to have a lower spin (0,1,2,3). The 2015-, 2030-, 2590-, 3424-, and 3510-keV levels only decay to the 236.5-keV 4^+ state. Those levels could have intermediate spins. The 2655-, 3596-, and 3660-keV levels are likely to have relatively high spins according to their decay patterns.

Figure 2 shows a γ-ray total spectrum from about 0 to 5 MeV. All the strong γ rays from ^{162}Gd as well as contaminations are labeled. The major contaminations of this experiment are from the decays of the mass 81 decay chain. The ^{126}Te contaminations are from the last experiment in this facility. Unknown contamination transitions from the residue of the past experiment and Fe are also labeled. A prompt-prompt γ-γ-ray matrix was built within a 1 μs time window, which is the time response of the prompt γ rays for the current Clover detectors. Figure 3 depicts a γ-ray coincidence spectrum by gating on the 164.8-keV transition in the g.s. band showing evidence for the new and previously reported transitions. In this gated spectrum, one can clearly see the 72-, 205-, 254-, 330-, 336-, 427-, 443-, 628-, 691-, 754-, 776-, 882-, 898-, 1007-, and 1257-keV transitions. Figure 4 denotes a gate on the 491-keV γ ray. The 103-, 122-, 142-, and 264-keV transitions in band (5) and the 791- and 863-keV transitions linking band (2) to band (1) can be seen. In the data analysis with the prompt-prompt γ-γ-ray matrix, most of the strong contaminations and scatter contaminations (labeled as "C" and "S" in Fig. 3) can be identified by simply doing background subtraction. In some complicated cases, e.g., transition energies are close to each other, those contaminations as well as real peaks can be identified by gradually changing the gated energy around the aiming gated energy and comparing the behavior of peaks in such a list of gated spectra. A strong contamination will keep the position and intensity as gated energy changes. A scatter contamination will keep the intensity but change the position of the peak in an opposite direction as gated energy changes. The strong contaminations and scatter contaminations are also discussed in the ^{164}Gd part.

In Ref. [13], a 1453-keV (6^-) state was reported without a lifetime measurement. This state is confirmed at 1449 keV as an isomer in the current work. The 205- and 330-keV transitions depopulating the 1449-keV level are strong in Fig. 2 but are almost not seen in the β-gated 1 μs prompt γ-ray spectrum. By summing the 205- and 330-keV transitions gated β to γ time decay curve (up to 1 ms), a constant plus exponential

FIG. 1. The new level scheme of ^{162}Gd obtained in the present work. New transitions and levels are labeled in red. The ^{162}Eu isomer energy is taken from Ref. [13].

decay is used to fit the half-life of the 1449-keV isomer. In the current work, the measured half-life of this isomer is 99(3) μs, as shown in Fig. 5.

Since the half-life of the 1449-keV level is measured, a proper β-gated prompt-delayed γ-γ matrix has been built to identify the transitions feeding this isomer. In the matrix, the

prompt γ-ray transition is defined from 0–1 μs after a β event, while the delayed γ ray is defined from 1–500 μs after the β event. The spectra of two gates on the delayed 330-keV γ ray and delayed 205-keV γ ray are shown in Fig. 6. In these two gates, one can see the strong 133- and 527-keV transitions as well as the weak 71-, 152-, 284-, and 755-keV transitions. The

TABLE II. The relative intensities (I_γ) of the γ-ray transitions in ^{162}Gd from the current experiment. The γ-ray intensities are normalized to the 164.8-keV transition. Tentative transitions are listed with parenthesis. The error bar is about 0.2 keV at 0 keV, 0.5 keV below 1 MeV, and 1 keV for transition energies above 1 MeV.

E_i (keV)	E_γ (keV)	I_γ (%)	E_f (keV)
71.7	71.7	29(3)	0
236.5	164.8	100(5)	71.7
490.1	253.6	51(3)	236.5
826.0	335.9	10(1)	490.1
863.0	791.4	27(3)	71.7
	862.9	22(1)	0
927.4	(64.4)	<1	863.0
	691.4	5.2(4)	236.5
	855.7	29(3)	71.7
1012.7	776.5	7.1(6)	236.5
	940.7	0.9(3)	71.7
1118.4	191.4	1.0(2)	927.4
	628.4	9.3(7)	490.1
	881.9	44(2)	236.5
1243.7	125	<0.5	1118.4
	230.7	0.8(1)	1012.7
	753.7	10(1)	490.1
	1007.1	7.5(6)	236.5
1354.2	341.9	1.4(2)	1012.7
	426.5	5.4(3)	927.4
	491.0	13(2)	863.0
1388.0	270.0	0.7(2)	1118.4
	898.2	3.5(4)	490.1
1427.8	1356.1	5.1(12)	71.7
1448.6[b]	205.2	8.9(5)	1243.7
	329.9	42(2)	1118.4
1457.1	102.7	2.6(6)	1354.2
	443.4	0.9(2)	1012.7
	529.8	2.0(4)	927.4
1493.1	1256.6	4.8(5)	236.5
1519.7	71.1	1.2(2)	1448.6
1579.3	122.2	2.2(7)	1457.1
1581.7	133.1	5.4(7)	1448.6
1645.3	152.2	0.1(1)	1493.1
	1408.8	<0.6	236.5
1701	838	1.5(5)	863.0
1714.8	133.1	0.4(1)	1581.7
1720.8	141.6	1.7(6)	1579.3
	264.5	1.1(3)	1457.1
1733.8	152.1	1.3(2)	1581.7
	284.0	0.8(2)	1448.6
1781	918	2.8(8)	863.0
1898.0	252.7	<0.6	1645.3
	1407.9	<0.6	490.1
	(1661.5)	<0.5	236.5
1975.4	526.8	9.7(5)	1448.6
2015	1778	1.5(4)	236.5
2030	1794	1.8(5)	236.5
(2148)	(2148)[a]	<3	0
2305	2233	5.7(19)	71.7
(2322)	(874)[a]	<2	1448.6
2337.2	755.5	1.4(4)	1581.7

TABLE II. (*Continued.*)

E_i (keV)	E_γ (keV)	I_γ (%)	E_f (keV)
2414	2342	2.5(12)	71.7
2418	2346	3.0(13)	71.7
2590	2354	1.2(4)	236.5
2655	2165	1.6(5)	490.1
3424	3187	2.6(7)	236.5
3510	3274	0.7(3)	236.5
3573	3501	4.9(20)	71.7
3596	2770	1.4(4)	826.0
	3106	3.4(9)	490.1
3660	(1339)[a]	<1	(2322)
	3170	2.1(6)	490.1
	3424	1.0(4)	236.5

[a]Not placed in the level scheme in Fig. 1.
[b]$t_{1/2} = 99(3)$ μs isomer; see Fig. 5.

placement of these transitions in the level scheme in Fig. 1 is based on their intensities in Fig. 6 and their coincidence relationship in the prompt γ-γ matrix.

Despite the weak transitions listed as tentative in Table II, some other transitions have ambiguous assignments and may belong to either mass = 79, 80, 81, or 162 nuclei. The 874- and 1339-keV transitions are in coincidence with each other. They are only seen in the 330-keV delayed γ gate, but not in the 205-keV delayed γ gate. Therefore, they are listed as tentative in Table II. The 2149-keV transition is not in coincidence with any γ ray in the current data. Close energy transitions at 2150 keV were reported in ^{81}Se in a ^{80}Se(n, γ) reaction [24]. This transition in ^{81}Se is not considered as the contamination because the coincidence transitions and transitions depopulating the same levels are not seen in the current work. The 3199-keV transition in Fig. 2 is in coincidence with 43 and 70 keV. The coincidence 70-keV energy is 2 keV away from the 72-keV γ ray in ^{162}Gd. The 3199-keV transition was also reported in ^{80}Se [25]. Although this transition is not reported in β-decay, it may weaken its evidence in ^{162}Gd. Thus, this transition is not placed in the level scheme in Fig. 1 nor in Table II.

The parent ^{162}Eu nucleus was reported to have a $\approx$160-keV isomer from a direct mass measurement in Refs. [13,26,27]. The ground state and the isomer of ^{162}Eu were assigned as $1^+ \pi 5/2[413] \otimes \nu 7/2[633]$ and $6^+ \pi 5/2[413] \otimes \nu 7/2[633]$, respectively [13]. The reported half-lives of ^{162}Eu were 10.6(10) s from Ref. [16], 11.8(14) s from Ref. [28], and 15.0(5) s Ref. [13]. To explain this difference, the author in Ref. [13] assumed different half-lives from the ground state and the isomer of ^{162}Eu populating low and high spins in ^{162}Gd, respectively. In the current work, different strong γ-ray gates were used to measure possible different half-lives. Note the ^{162}Sm nucleus half-life was reported as 2.4(5) s from the β-decay study in Ref. [29] with 36.0-, 736.7-, and 741.1-keV transitions assigned to the daughter ^{162}Eu nucleus. The current data do not show evidence for these three transitions neither in the γ-ray total in Fig. 2, nor in the β-gated γ-ray spectra. Thus, the half-life measurements in the current work do not
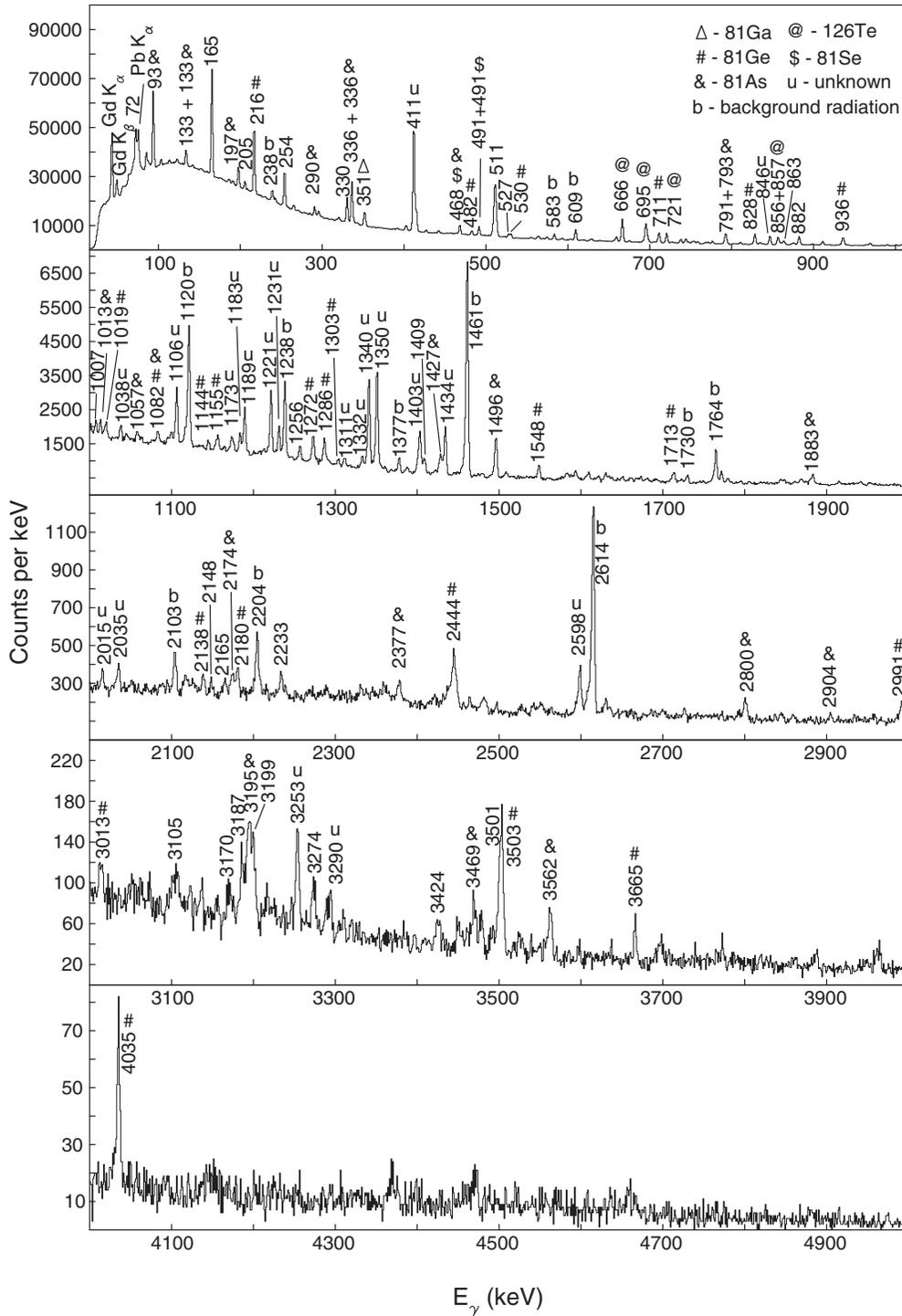
FIG. 2. The γ-ray total spectrum in ^{162}Gd. Here unknown contamination γ rays labeled with "u" are weak or not in coincidence with a β ray. They are possibly from Fe isotopes. Some of the small peaks in the spectrum are weak and not in coincidence with known γ rays. The origin of those peaks are not clear and thus not labeled in the spectrum.

have influence from ^{162}Sm. The half-lives were fitted to grow-decay curve using the same equation as in Ref. [22] Eq. (1):

$$I_0(t) = \begin{cases} A_0(1 - e^{-t/\tau_0}), & 0 < t < t_1, \\ A_0(e^{t_1/\tau_0} - 1)e^{-t/\tau_0}, & t_1 < t < t_2. \end{cases} \quad (1)$$

Here $t_1 = 22s$ and $t_2 = 44s$ for tape cycle settings in ^{162}Gd. The measured results are shown in Fig. 7 and Table III. The 205- and 330-keV gates should give the half-life of the possible high spin state of ^{162}Eu. The 165- and 253-keV gates were also used to compare to the result in Ref. [13]. These results do
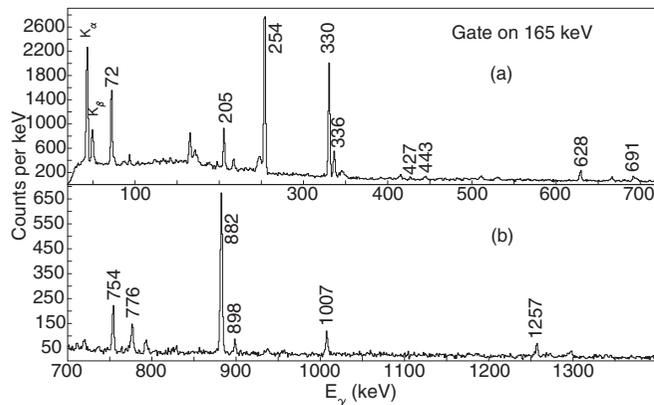
FIG. 3. Partial γ-ray coincidence spectrum by gating on the 164.8-keV transition in ^{162}Gd in the prompt γ-γ matrix.

not show a clear difference in the half-lives. From the intensity measurement in Table II, direct β feeding contributes $\approx 70\%$ of the 863-keV-level γ-ray (791 and 863) intensities. Only the 863-keV gate was used in the current work, because the 791 keV is strongly contaminated by the 793-keV transition (more than half of the peak in Fig. 2) in ^{81}As. The result for the 863 gated half-life is consistent with the other gates discussed above. The 856-keV transition is contaminated by the 857-keV transition in ^{126}Te. The measured value of 10.8(5) s for 72-keV transition shows some difference from the other gates used in the present work. Such difference may be due to contamination of the 73-keV $K_{\alpha 2}$ of Pb. The 43-keV K_{α} x ray of the Gd gate is also used for comparision. The Tb element also has a 44-keV K_{α}, but the contribution can be neglected, for the reason discussed below. The strong 403-, 442-keV transitions in ^{162}Tb reported in Ref. [19] are $\approx 4.5\%$ and 5.3% of the 165-keV transitions in ^{162}Gd in the total γ-ray spectrum in Fig. 2, respectively. These ^{162}Tb transitions are weak in the spectrum and do not generate significant internal conversion with x rays. In all, the result from the present work does not show evidence for two different half-lives in ^{162}Eu. It is possible that the reported [13] 160.2(24)-keV isomer in ^{162}Eu only decays to the ground state of ^{162}Eu, or the half-lives of the two state in ^{162}Eu are very close. The former one is not quite
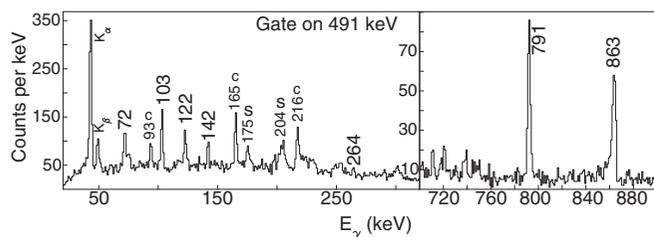
FIG. 4. Partial γ-ray coincidence spectrum by gating on the 491.0-keV transition in ^{162}Gd in the prompt γ-γ matrix. In the spectrum, "c" stands for a contamination transition which is strong and in coincidence with any gated energy in this region. The "s" stands for a scattering contamination when a γ ray scatters from one detector to another. For a scattering contamination, the sum of gated energy and the scattering energy is equal to a strong transition energy.
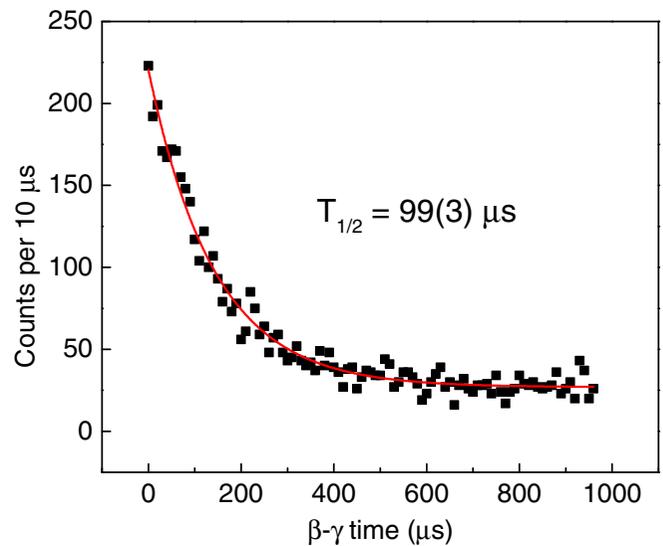
FIG. 5. Halflife measurement of the (6$^-$) 1449-keV level. The x axis is the time difference between the β and the 205-, 330-keV transitions.

possible as discussed below. The possible 160-keV isomeric transition in ^{162}Eu is not seen in our data. The data do show some very weak evidence for a 103–57 keV coincidence and a 99–61 keV coincidence. However, they are not considered as the cascades linking the 160-keV isomer and the ground state in ^{162}Eu because of the lack of confirmation in previous ^{162}Sm β decay to ^{162}Eu data.

B. ^{164}Gd

A newly developed level scheme for ^{164}Gd is shown in Fig. 8 with 16 new transitions, 13 new levels, and 2 transitions that were previously observed [16] now, for the first time, placed into the level scheme. Table IV denotes the list of
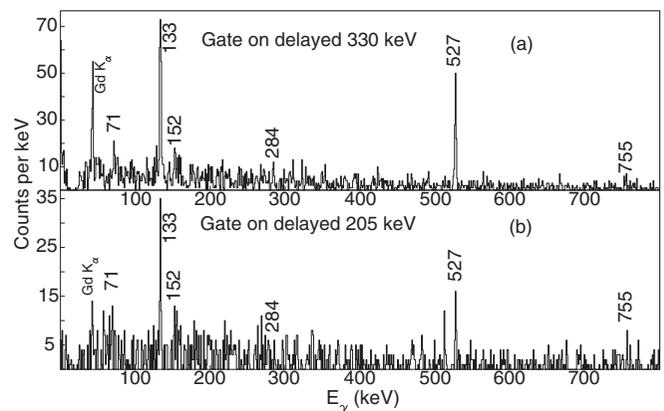
FIG. 6. Partial background subtracted γ-ray coincidence spectra (a) by gating on the 329.9-keV delayed transition, and (b) by gating on the 205.2-keV delayed transition in ^{162}Gd in the β-prompt-delayed asymmetric γ-γ matrix. In this matrix, the prompt γ-ray transition is defined from 0–1 μs after a β event, while the delayed γ ray is defined from 1–500 μs after the same β event.
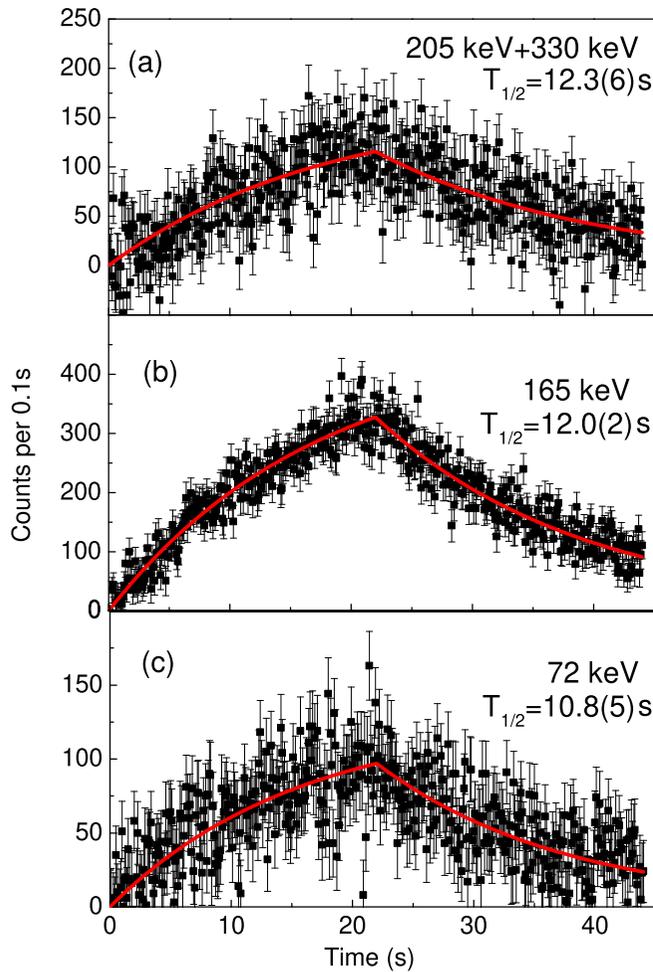
FIG. 7. Growth and decay fitting for ^{162}Eu half-life from background subtracted (a) 205- and 330-keV gate, (b) 165-keV gate, and (c) 72-keV gate. Note that the 72-keV gate is contaminated by the Pb x ray.

the γ-ray energies, intensities, initial and final levels, and tentative spin-parity assignments. The ^{164}Eu parent nucleus is weaker populated in the beam than ^{162}Eu which results in a slightly different data analysis process.

TABLE III. Table of the half-lives of ^{162}Eu by gating on different γ rays. The results are compared with previous experimental data.

Reference	Gates	Eu half-life (s)	Depopulating spin
[17]	K x ray	10.6(10)	
[28]	ion-β	11.8(14)	
[13]	165, 254	15.0(5)	$4^+, 6^+$
This work	205, 330	12.3(6)	(6^-)
	165	12.0(2)	4^+
	254	11.6(4)	6^+
	863	11.7(12)	2^+
	72[a]	10.8(5)	2^+
	43 (K_α)	11.6(3)	

[a]This gate is contaminated.

First, the ^{164}Gd data were compiled using a 1 μs coincidence window, which is the same coincidence time as the prompt event matrix in ^{162}Gd. Figure 9 shows the γ-ray singles and β-gated γ-ray singles. First the singles spectrum is generated by every γ-ray interaction with any of the 16 HPGe crystals in the 4 clovers of the LeRIBSS station with no coincidence of any kind required. In this single spectrum, all but the weakest peaks from ^{164}Gd can be seen, as well as the greatest number of contamination peaks. The way of generating this spectrum is the same as the one in Fig. 2 in ^{162}Gd. Second, the β-gated singles are just like the singles except that any γ ray recorded in the spectrum must be in coincidence with a β ray. This drastically reduces the contaminant peaks, as shown in the ^{162}Gd part before, and enhances the peak to background ratio of many of the peaks in which we are interested.

The spectra in Fig. 10 are both from background subtracted gates on γ rays, with no requirement of β coincidence. Both of these coincidence spectra use add-back, where any γ-ray interactions in different crystals of the same clover are added back together under the assumption that they were in fact the same original γ ray. The background subtraction in these gates was done by subtracting gates on channels immediately to the left and right of the desired gate energies from the desired channels. Part (a) is a spectrum gated on the 169-keV transition in the ground state band, showing the clear 73-, 92-, 193-, 793-, 854-keV known transitions and new 261-, 301-, and 1081-keV transitions. Part (b) is a spectrum gated on the 854-keV transition, in which the 93-, 193-, and 301-keV transitions feeding the isomer can be clearly seen. The add-back background subtracted gate does not remove Compton scatter events, when a higher energy γ-ray Compton scatters into a different clover detector. These scatter events create diagonal lines in the 2D histogram from which these gates were taken, meaning that the background gates see the scatter peak at higher or lower energy than the gate energies and create sharp negative peaks in the final spectrum on either side of the cross talk peak, making them easier to spot. Scatter peaks are labeled with an S in Fig. 9.

The most prominent contaminants in our data are from the $A = 82$ and 81 chains. Transitions from these nuclei have been marked with triangles in Fig. 9. We end up with $A = 81$ nuclei in our data from $\beta - n$ decay. Further details on the γ rays produced by these $A = 81, 82$ contaminants can be found in references [30–35].

A number of contaminant γ rays exhibit one distinguishing feature in common; that they experience no coincidence with other γ rays or β particles. These contamination γ rays can be confirmed by comparing the spectra from ^{162}Gd in Fig. 2 and ^{164}Gd. These have been marked with a letter b in Fig. 9. These coincidence-less peaks also show no time variation behavior, meaning that they cannot be contained in our beam or dependent on our tape cycle. One contaminant which can be identified is ^{126}Te (stable residue and Coulomb excited), due to its obvious coincidence relationships and well known energy structure [36,37]. The transitions from ^{126}Te are marked by an "@" symbol in Fig. 9. Additionally, the Pb x rays are from the activated Pb bricks used to shield the
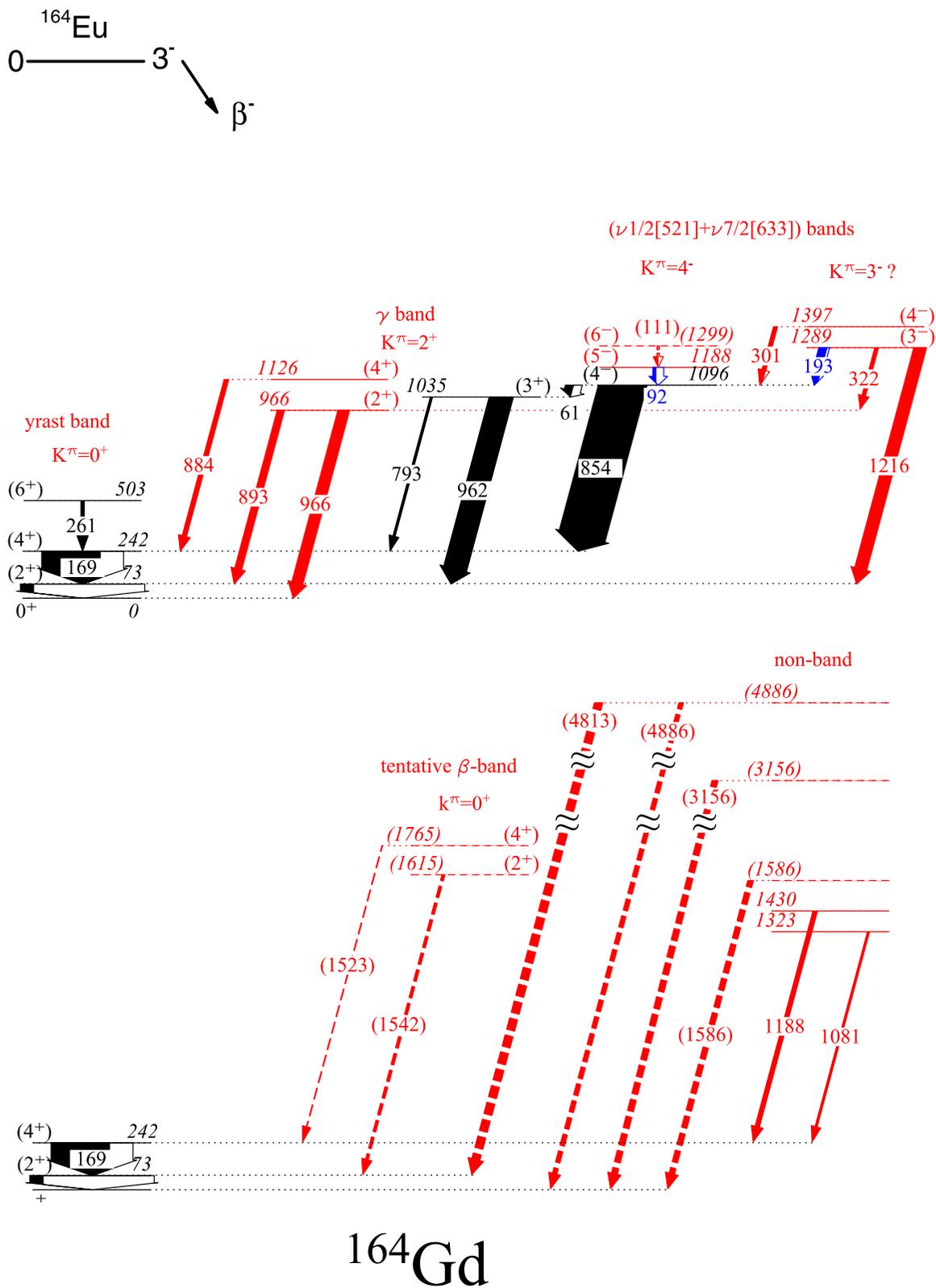
FIG. 8. The level scheme of ^{164}Gd as seen by the β decay of ^{164}Eu. Red levels and transitions are newly observed in this work. Blue transitions are previously observed [16] but had not been placed in the level scheme. Other previously reported transitions are labeled in black.

TABLE IV. Table of levels and γ rays in ^{164}Gd. Square brackets indicate that a value is tentative. Subscripts on spin-parity labels indicate band. Here E_i is the level energy populating the γ rays and E_f is the level populating the γ rays.

E_γ	I_γ	ΠL	E_i	J_i^π	E_f	J_f^π
61.0[d]	13(3)	E1	1095.7[a]	$[4_4^-]$	1034.7	$[3_\gamma^+]$
72.9	23(6)	[E2]	72.9[b]	$[2_g^+]$	0.0[c]	0_g^+
91.6[d]	5(2)	[M1]	1187.3	$[5_4^-]$	1095.7[a]	$[4_4^-]$
[110.7][e]	1.6(13)	[M1]	[1298.0]	$[6_4^-]$	1187.3	$[5_4^-]$
168.5	100(6)	[E2]	241.4	$[4_g^+]$	72.9[b]	$[2_g^+]$
192.8[d]	13(2)	[M1]	1288.5	$[3_3^-]$	1095.7[a]	$[4_4^-]$
260.7	5.3(9)	[E2]	502.1	$[6_g^+]$	241.4	$[4_g^+]$
300.8[e]	11(4)	[M1]	1396.5	$[4_3^-]$	1095.7[a]	$[4_4^-]$
322.2[e]	8(4)	[E1]	1288.5	$[3_3^-]$	966.3	$[2_\gamma^+]$
793.3	3.7(15)		1034.7	$[3_\gamma^+]$	241.4	$[4_g^+]$
854.3	81(7)		1095.7[a]	$[4_4^-]$	241.4	$[4_g^+]$
883.9[e]	8(2)		1125.3	$[4_\gamma^+]$	241.4	$[4_g^+]$
893.4[e]	12(2)		966.3	$[2_\gamma^+]$	72.9[b]	$[2_g^+]$
961.8	40(4)		1034.7	$[3_\gamma^+]$	72.9[b]	$[2_g^+]$
966.3[e]	19(6)		966.3	$[2_\gamma^+]$	0.0[c]	0_g^+
1080.8[e]	3.5(14)		1322.2		241.4	$[4_g^+]$
1187.8[e]	7(2)		1429.2		241.4	$[4_g^+]$
1215.6[e]	21(3)		1288.5	$[3_3^-]$	72.9[b]	$[2_g^+]$
[1523.5][e]	<5		[1764.9]	$[4_4^+]$	241.4	$[4_g^+]$
[1542.5][e]	<17		[1615.4]	$[2_\beta^+]$	72.9[b]	$[2_g^+]$
[1585.7][e]	9(6)		[1585.7]		0.0[c]	0_g^+
[3156.3][e]	10(4)		[3156.3]		0.0[c]	0_g^+
[3789.8][f]	<10					0_g^+
[4812.6][e]	14(6)		[4885.5]		72.9[b]	$[2_g^+]$
[4885.5][d]	8(4)		[4885.5]		0.0[c]	0_g^+

[a]Isomeric state: $t_{1/2} = 0.56(3)\,\mu$s, see Fig. 11.

[b]2^+ state half-life: $t_{1/2} = 2.77(14)$ ns [38].

[c]Ground state half-life: $T_{1/2} = 45(3)$ s [39].

[d]Reported in [16] but not placed in the level scheme.

[e]Newly observed transitions in this work.

[f]Not placed in the level scheme.

LeRIBSS station. The x rays of Pb are marked by circles in Fig. 9.

The intensities displayed in Table IV were measured using both the total γ-ray spectrum and the gated γ-ray coincidence spectra, as shown in Figs. 9 and 10. The first spectrum is the γ-ray singles spectra, which displays all γ rays detected during the nearly two hours of data collection, with no coincidence requirement or attempt to correct for losses due to effects like internal conversion. The second spectrum used was the β-gated singles, which is the same as the singles spectrum but has the added restriction that any γ ray included must be in coincidence with at least one electron, which reduces several sources of background contamination. The third and fourth spectra were background-subtracted gates on the 168.5- and 854.3-keV γ rays, respectively. Both the singles, and β-gated singles were normalized such that the intensity of the 168.5-keV γ ray was 100. The gate on 168.5 keV was normalized so that the 854.3-keV γ ray was equivalent to what was measured in the singles spectrum. The 854.3-keV gate was normalized by the intensity of the 192.8-keV γ ray, compared to its weighted average intensity in both the singles and β-gated singles spectra. In the single total spectra some transitions were contaminated by the mass 81, 82 transitions or too weak to measure, and hence the γ-ray gated spectra were used to obtain the energies and intensities. However, transitions populating the 1095-keV isomer would be attenuated when gating on transitions below it and result in some uncertainty.

The internal conversion coefficient of the 61.0-keV transition was measured by comparing the 61.0-, 793.3-, and 961.8-keV γ-ray intensities in the 192.8-keV transition gate above the isomer. The sum of the gated intensities of the two transitions depopulating the 1034.7-keV state fed by the 61.0-keV transition are taken as the total gated intensity $(\gamma + e^-)$ of the 61.0-keV transition. This gated intensity is compared to the measured gated intensity of the 61.0-keV γ-ray transition. This means that the internal conversion coefficient of this 61.0-keV transition is

$$\alpha_{61} = \frac{I_{961} + I_{793}}{I_{61}} - 1, \qquad (2)$$
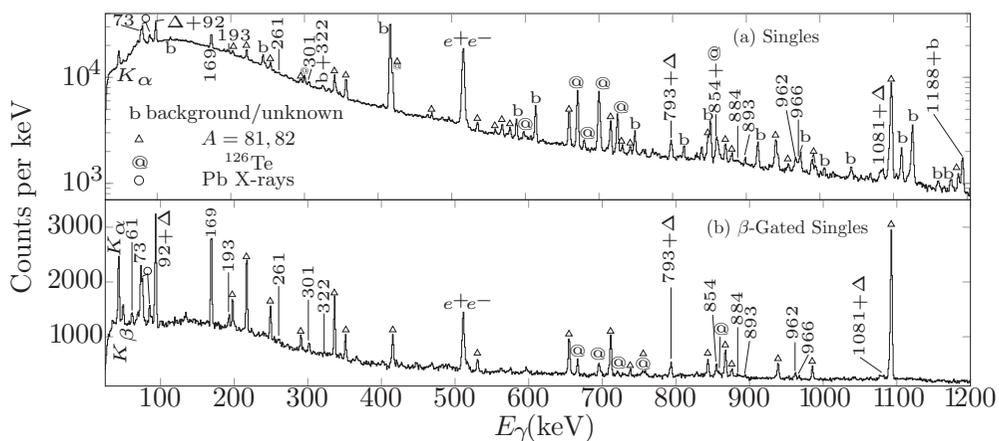
FIG. 9. Spectra from the LeRIBSS ^{164}Eu β-decay data for (a) γ-ray singles, (b) β-gated γ-ray singles.
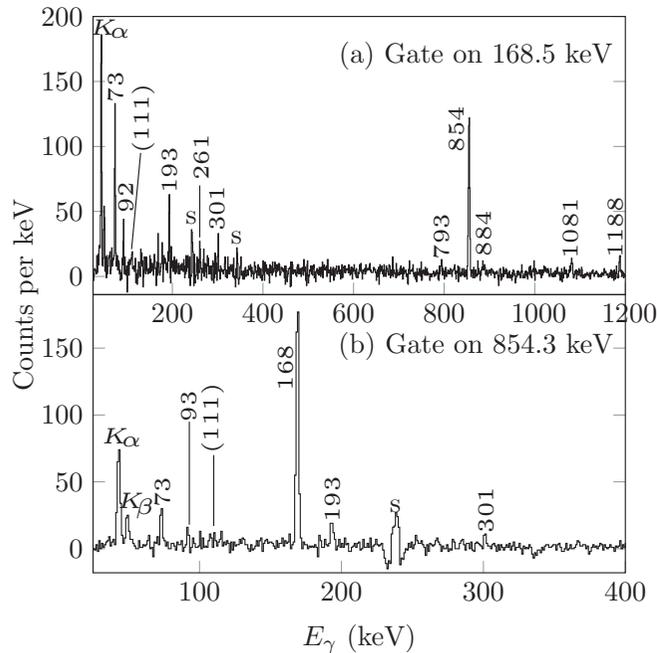
FIG. 10. Spectra from the LeRIBSS ^{164}Eu β-decay data for (a) a background subtracted gate on the 168.5-keV γ ray, (b) a background subtracted gate on the 854.3-keV γ ray.

where α is the internal conversion coefficient and I is the measured γ-ray intensity of a transition. The one complication to this is that, in the 192.8-keV gate, the 793.3-keV transition is barely identifiable above background, and thus too weak to fit. The branching ratios of the 793.3- and 961.8-keV transitions from the total γ-ray intensities in Table IV were used to determine the intensity of the 793.3-keV transition. These measured intensities of the 962- and 61-keV transitions and the calculated intensity of the 793-keV transition in this background subtracted 192.8-keV gate are used to deduce the internal conversion coefficient of the 61-keV transition. The experimentally measured internal conversion coefficient for this transition is 1.0(7). By comparing to the theoretical value for 1.1 E1, 8.4 M1, and 17 E2 in Ref. [40], the 61-keV transition is determined to be an E1 transition by brIcc [40].

The lifetime of the 1095.7-keV state has been measured to be 0.56(3) μs. This measurement was conducted by measuring the exponential decay rate from the $\beta - \gamma$ time, or the time between the detection of an electron and the detection of a γ ray, by using a 2 μs rolling coincidence for longer observation of the isomer. In the $\beta - \gamma$ time versus γ-ray energy plot, the sum of the 854.3- and 168.5-keV γ rays was used for this measurement. The resulting summed gate is displayed in Fig. 11. In Fig. 11, first is the large sudden rise and rapid drop caused by fundamental limitations of our detector crystals. The second feature is caused by the decay of the isomer. An exponential decay fit was performed, which appeared as a straight line on a logarithmic graph, as seen in Fig. 11. This section of the graph has been fit to determine the lifetime of the 1095.7-keV state. The third segment of Fig. 11 is the appearance of a shorter lifetime starting at 2 μs. This effect is caused by the nature of the "rolling" coincidence by
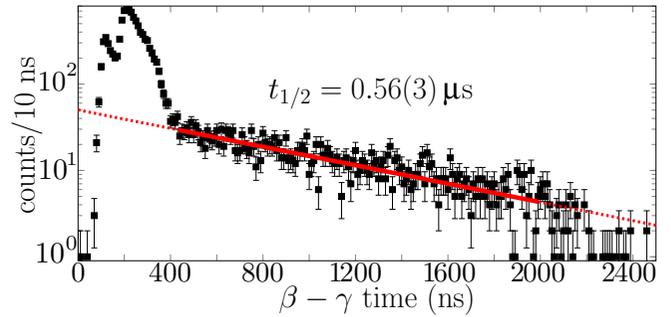
FIG. 11. A plot of sum of gates on the 854.3- and 168.5-keV γ-ray energies as a function of the $\beta - \gamma$ time. The data were recompiled using a 2 μs rolling coincidence window for the lifetime measurement. The fit shown between the end of the "bump" at $\approx$400 ns and 2 μs is used to determine the lifetime of the 1095.7 (4$^-$) isomer in ^{164}Gd.

which our data were compiled. This section was not included in the fit to determine the lifetime of the 1095.7-keV state.

Finally, the lifetime of the ^{164}Eu β-decay parent of ^{164}Gd has been measured by examining the tape cycles, as shown in Fig. 12. A 2D histogram was generated which gives γ-ray energy versus time within a tape cycle, and consists in the sum of all tape cycles. As noted in the experimental setup section, the tape cycle was 8 s beam-on, followed by 8 s beam-off, for a total of 16 s. This means that our total tape cycle is only about 4 half-lives (previous: 4.2(2) s [16] and 3.80(56) s [28], see also Ref. [39]), with only two half-lives being allowed for each grow-in and decay-out, which increases the uncertainty in this lifetime measurement. While only 2 half-lives is shorter than desired for the measurement of the ^{164}Eu half-life, it does minimize some the presence of contaminants from our beam. For example, it mostly precludes population of ^{164}Tb from the β-decay of ^{164}Gd, as that half-life is 45(3) s [41]. Background
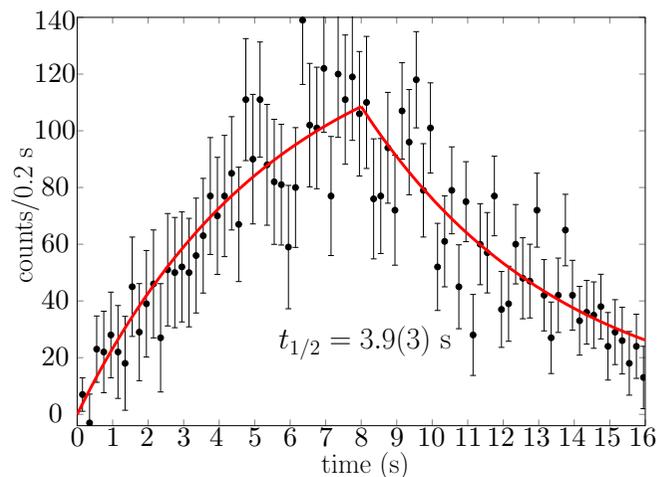
FIG. 12. A plot of the measurement of the β-decay half-life of ^{164}Eu. Requiring β-coincidence, background subtracted γ-ray gates on 72.9, 168.5, and 854.3 keV were summed to produce the time spectrum below. The grow-in and decay-out were fit simultaneously to produce the curves shown. The resulting half-life is 3.9(3) s.

subtracted gates on 72.9-, 168.5-, and 854.3-keV transitions were combined for more statistics. Both the grow-in and decay out were fit simultaneously with a piecewise function as also stated in Eq. (1) in Ref. [22]. From this fit we deduced the half-life of ^{164}Eu to be 3.9(3) s, in agreement with the 4.15(20) s NNDC accepted half-life [39]. The result of these gates and fitting is shown in Fig. 12.

IV. DISCUSSION

A. J^π assignments of ^{162,164}Eu

The β-feeding of levels in ^{162}Gd can be deduced from the γ-ray decay in and out intensity balance. The calculated values for strongly populated levels are 72-keV 2^+, 65(30); 236-keV 4^+, 9(8); 490-keV 6^+, 16(3); 863-keV 2^+, 31(4); 927-keV 3^+, 26(3); 1448-keV 6^-, 21(3). In the calculation, the 64.4 tentative γ ray is neglected with upper limits or intensities. Meanwhile, the 71.1-keV transition is treated as a pure M1 for internal conversion calculation. Choosing other E1 or M1/E2 mixed internal conversion values would also give a large feeding of the 1448-keV state. The accurate percentage of β feeding cannot be obtained because of the possibility for two different ^{162}Eu branches. The ground state β feeding can be calculated from the ^{162}Gd and the daughter ^{162}Tb counts ratio. From Eq. (1), the number of the created ^{162}Gd atoms is

$$N(^{162}\text{Gd}) = \int_{t_1}^{t_2} I_0(t)dt. \quad (3)$$

Here taking $T_{1/2} = 11.8$ s, which is the weighted average of the measurements of gating on 43-, 165-, 254-, 205+330-, 863-keV transitions by neglecting the possible difference between the β-decay half-lives of the ^{162}Eu ground state and 160-keV isomer, one obtains $\tau_0 = T_{1/2}/\ln(2) = 17.0$ s and $N(^{162}\text{Gd}) = 18.616A_0$ [A_0 is defined in Eq. (1)]. Similar to the equation in Ref. [22], the total number of ^{162}Gd atoms left during the tape cycle without decay is the integral

$$N(^{162}\text{Gd})_R = \int_0^{t_2} e^{-(t_2-t)/\tau'} I_0(t)dt. \quad (4)$$

Taking a weighted average from Refs. [18,19], $T_{1/2}(^{162}\text{Gd}) = 503s$, one can get $\tau' = T_{1/2}(^{162}\text{Gd})/\ln(2) = 725$ s. The integral is $N(^{162}\text{Gd})_R = 18.062A_0$. The number of ^{162}Tb atoms created from decay is the difference of these two $N(^{162}\text{Tb}) = N(^{162}\text{Gd}) - N(^{162}\text{Gd})_R = 0.554A_0$. Thus, $N(^{162}\text{Gd})/N(^{162}\text{Tb}) = 33.6$. The $N(^{162}\text{Tb})$ can be evaluated by adding the 403- and 442-keV transition intensities depopulating the 442-keV level, which has 95.5% β-feeding according to Ref. [19]. This value times the 33.6 factor can give the $N(^{162}\text{Gd})$ value. The $N(^{162}\text{Gd})$ contains 72-, 863-keV ground-state γ rays and ground-state β feeding. By doing the subtraction, the ^{162}Gd ground-state β feeding is 34 (39) (not percentage). This value would be an upper limit for possible ^{162}Gd in the beam. To explain the relatively strong β feeding of the 2^+, 3^+, 4^+, 6^+, 6^- ^{162}Gd states, we propose the ^{162}Eu ground state and 160-keV isomer to be 6^+ $\pi5/2[413] \otimes \nu7/2[633]$ and 3^- $\pi5/2[413] \otimes \nu1/2[521]$, respectively, by comparing with the neighboring nuclei $N = 99$ $\nu7/2[633]$ ground state for ^{161}Sm [11,42], ^{163}Gd [43], ^{165}Dy [44]; $Z = 63$ $\pi5/2[413]$ ground state for ^{159}Eu [45];

TABLE V. The γ-ray feeding, outflow, and β feeding of excited levels in ^{164}Gd from the β decay of ^{164}Eu calculated from Table. IV. Ground-state β feeding is assumed to be 0. Note the weakly populated levels are not accurate because of the possible unobserved high-energy transitions due to low yield of population and low efficiency. Subscripts on spin-parity labels indicate their band, either a simple identifier for collective bands or the value of K for the quasiparticle bands.

E_{level} (keV)	I^π	γ feeding	γ outflow	Iβ	Iβ (%)	log(ft)
0.0	0^+_g	261(57)	0	≈0	≈0	
72.9	$[2^+_g]$	232(16)	214(61)	<46	<18	>6.3
241.4	$[4^+_g]$	108(8)	140(8)	31(11)	12(4)	6.4(2)
502.1	$[6^+_g]$	0	5.8(10)	5.8(10)	2.2(4)	7.1(1)
966.3	$[2^+_\gamma]$	8(4)	31(6)	24(7)	9.2(27)	6.3(2)
1034.7	$[3^+_\gamma]$	28(7)	43(4)	16(13)	6.1(50)	6.5(4)
1095.7	$[4^-_4]$	47(8)	108(14)	61(16)	23(6)	5.9(2)
1125.3	$[4^+_\gamma]$	0	8(2)	8(2)	3.1(8)	6.8(1)
1187.3	$[5^-_4]$	4(3)	18(6)	14(7)	5.4(27)	6.5 (3)
1288.5	$[3^-_3]$	0	47(6)	47(6)	18(2)	5.9(1)
[1298.0]	$[6^-_4]$	0	4(3)	4(3)	1.5(11)	7.0(4)
1322.2		0	3.5(14)	3.5(14)	1.3(5)	7.0(2)
1396.5	$[4^-_3]$	0	12(4)	12(4)	4.6(15)	6.5(2)
1429.2		0	7(2)	7(2)	2.7(8)	6.7(2)
[1585.7]		0	9(6)	9(6)	3.4(23)	6.5(4)
[1615.4]	$[2^+_\beta]$	0	<17	<17	<6.5	>6.2
[1764.9]	$[4^+_\beta]$	0	<5	<5	<2	>6.7
[3156.3]		0	10(4)	10(4)	3.8(15)	5.7(2)
[4885.5]		0	22(7)	22(7)	8.4(27)	4.1(2)

and $N = 99$ $\nu1/2[521]$ isomer in ^{163}Gd [43,46] 138-keV 23.5(10) s, ^{165}Dy 108-keV 1.257(6) min [44].

From the intensity data shown in Table IV, we can calculate the combined β and γ feeding for each level in ^{164}Gd. The results of this analysis are shown in Table V. Since the known Q value for the β decay of ^{164}Eu is 6.39(5) MeV [47], it seems likely that other weak high-energy states and γ rays are produced in the β decay of ^{164}Eu which remain unobservable in our data due to the low efficiencies of the HPGe detectors at higher energies. Thus, the current β-feeding measurements and the determined log(ft) values for ^{164}Gd are only valid and referable for strong β-feeding levels. However, we can still attempt to deduce the spin and parity of the ground state and β-decaying isomers of ^{164}Eu. Since the relatively reliable spins of 241-keV 4^+, 966-keV (2^+), 1035-keV (3^+), 1096-keV (4^-) states receive strong feeding, $3^\pm$ and 4^- are preferred for the ground state of ^{164}Eu. The log(ft) value for the 1095.7 (4^-) state lies on the edge of an allowed transition. Thus, 3^- and 4^- are more favored. The 1187-keV (5^-) level also receives strong β-feeding, but the value is not very reliable due to the strong contamination of the 93-keV transition from ^{81}As. The proton and neutron Nilsson orbitals near the fermi energy are $\pi5/2^+[413]$, $\pi5/2^-[532]$, $\pi3/2^+[411]$, $\nu1/2^+[521]$, and $\nu7/2^+[633]$. The only combination is $3^-\pi5/2[413] \otimes \nu1/2[521]$. This assign-

ment is consistent with the tentative assignment from nuclear data sheets (Ref. [39]).

B. High *K* quasiparticle states and hindrance

According to Patel *et al.* [11] and Yokoyama *et al.* [9] (same research group), the decay of the 1095.7-keV level in ^{164}Gd is hindered by a large change in *K*. For the 854-keV γ ray, $\Delta K = -4$, even though $\Delta J = 0$. An experimental hindrance factor can be defined as $f_\nu \equiv (t_{1/2}^\gamma / t_{1/2}^W)^{1/\nu}$, where $t_{1/2}^W$ is the Weisskopf predicted half-life for the transition, $t_{1/2}^\gamma$ is the γ-ray partial half-life, $\nu = |\Delta K| - L$, and *L* is the multipole order of the transition (i.e., *EL* or *ML*). Patel *et al.* [11] reports $f_3 = 1.4 \times 10^3$ for the 854-keV γ ray, while Yokoyama *et al.* [9] quotes $f_3 = 1.28(3) \times 10^3$. The difference between these two results primarily stems from differing branching ratios of the 61-keV transition compared to the 855-keV γ ray. The present experiment has better statistics than either Patel *et al.* or Yokoyama *et al.*, and a new half-life measurement which is consistent with both of their half-life measurements. Based on these considerations we have found $f_3 = 1.27(7) \times 10^3$ for the 854-keV transition and $f_1 = 4.5(13) \times 10^6$ for the 61-keV transition. The current independent measurement confirms the measurements of Yokoyama *et al.* with $f_3 = 1.28(3) \times 10^3$. These two hindrance factors were measured with partial half-lives $t_{1/2}^\gamma(61) = 4.5(13)\,\mu$s, $t_{1/2}^{IC}(61) = 4.1(36)\,\mu$s, and $t_{1/2}^\gamma(854) = 0.75(12)\,\mu$s, derived from the branching ratios of the 854- and 61-keV γ rays and the ICC of the 61-keV transition. For ^{162}Gd, the hindrance factor of the 330-keV transition depopulating the 1449-keV (6^-) isomer can also be obtained for comparison. With $\Delta K = 4$, $\nu = 1$, and $t_{1/2} = 99(3)\,\mu$s, the calculated f_ν is 2325(23). This value is not only larger than the ^{164}Gd 4^- value, but also significantly larger than the E1 transitions depopulating the 6^- $\nu 5/2[512] \otimes 7/2[633]$ isomer in ^{164}Sm $f_\nu = 487(38)$, ^{166}Gd $f_\nu = 356(7)$ reported in Ref. [12]. A 6^- $\nu 5/2[523] \otimes 7/2[633]$ $t_{1/2} = 339(20)$ns isomer was reported in ^{158}Nd [7]. The 1197-keV E1 transition (followed by 233- and 152-keV transitions) decaying from the ^{158}Nd isomer to the ground-state band leads to a factor $f_\nu = 76(1)$. From the current calculation as discussed later, the 1449-keV 6^- isomer in ^{162}Gd is also proposed to be 6^- $\nu 5/2[523] \otimes 7/2[633]$. Such differences may indicate that the 152-, 233-, 1197-keV transitions reported in Ref. [7] in ^{158}Nd were wrongly placed—the correct order may be 152-keV $4_g^+ \to 2_g^+$, 1197-keV $5_\gamma^+ \to 4_g^+$, and 233-keV $6^- \to 5_\gamma^+$. Such an assignment gives $f_\nu = 264(5)$ and is generally close to the values in ^{164}Sm and ^{166}Gd.

By using the intensity data in Table IV, the $B(\Pi L)$ ratios can be determined for the transitions out of the 966.3-, 1034.7-, 1095.7-, and 1288.5-keV levels in ^{164}Gd. All of the measured ratios are presented in Table VI.

The assignment about the 1288.5-keV level in ^{164}Gd can be made based on the $B(\Pi 1)$ ratios and final spin-parity of its three depopulating γ rays. First, it decays to the 72.9-keV 2_g^+, 966.3-keV (2_γ^+), and 1095.7-keV (4_4^-) states, thus its own spin and parity must be 2^-, $3^\pm$, or 4^+, because only *M*1, *E*1, and *E*2 transitions are commonly observed. Second, the

TABLE VI. Reduced transition probability ratios measured for ^{164}Gd as seen by the β decay of ^{164}Eu. Subscripts on spin-parity labels indicate band, either a simple identifier for collective bands or the value of *K* for the quasiparticle bands.

γ-ray decay pattern	Ratio
$B(E2; 966; 2_\gamma^+ \to 0_g^+)/B(E2; 894; 2_\gamma^+ \to 2_g^+)$	1.1(3)
$B(E2; 962; 3_\gamma^+ \to 2_\gamma^+)/B(E2; 793; 3_\gamma^+ \to 4_g^+)$	4.1(17)
$B(E1; 854; 4_4^- \to 4_g^+)/B(E1; 61; 4_4^- \to 3_\gamma^+)$	0.0027(7)
$B(E1; 1216; 3_3^- \to 2_g^+)/B(E1; 322; 3_3^- \to 2_\gamma^+)$	0.05(3)
$B(E1; 1216; 3_3^- \to 2_g^+)/B(M1; 193; 3_3^- \to 4_4^-)$	0.0063(13)
$B(E1; 322; 3_3^- \to 4_4^-)/B(M1; 193; 3_3^- \to 4_4^-)$	0.12(7)

reduced transition probabilities of the 192.8- and 322.1-keV transitions are clearly much higher than that of the 1215.6-keV transition in Table VI, which favors a high *K* for the 1288.5-keV level. By comparing with the reduced transition probability ratios found in Lesher *et al.* [48] for ^{160}Gd, nearly all collective states can be rule out. In Lesher *et al.*, the levels of the γ-vibrational band of ^{160}Gd decay only to the ground state band, while the 1288.4-keV state in ^{164}Gd is observed decaying to both γ-vibrational and ground-state bands. Furthermore, the energy space for the 1288.5-keV state does not match for it to be a γ-vibrational state. One can also rule out $K^\pi = 0^-$, 1^- octupole vibrational bands, as they are also observed to only decay to the ground state band in ^{160}Gd by Lesher *et al.* The most likely option by observing Lesher *et al.* is the 3^- of a 2^- octupole vibrational band. Lesher *et al.* observes this state in ^{160}Gd decaying to the 4_γ^+, 3_γ^+, and 2_γ^+ with about equal intensities and the 4_g^+ with about 0.7% the reduced transition probability of the other transitions from this level. We rule this level out for ^{164}Gd, because we observe it decaying only to the 2_γ^+ instead of all three γ-vibrational states, and observe decay to the 2_g^+ state, rather than the 4_g^+ state. The 1288.5-keV level cannot be the 4_β^+ level, as decay from this state to the γ-vibrational band would be forbidden, as it simultaneously would create a γ phonon while destroying a β phonon. This statement assumes no β-γ mixing (i.e., $Z_{\beta\gamma} = 0$), and may not be true. However, comparison with the β band of ^{160}Gd cited in Lesher *et al.*, indicates that the assumption of no decay from the β band to the γ band holds true for neutron-rich, even-even Gd isotopes. Thus, the 1288.5-keV level is most likely to be a quasiparticle state. According to its almost allowed log(ft) value, 2^-, 3^-, and 4^- are the most probable candidates. Combining with the decay pattern discussed above, we believe that the 1288.5-keV level is likely a 3^- $\nu 1/2[521] \oplus \nu 7/2[633]$ state and favors decay to the 1095.7, (4^-) level due to the shared configuration. The assignment of this configuration is in consistent with the 1094-keV 4^- $\nu 1/2[521] \oplus \nu 7/2[633]$ isomeric state reported in ^{168}Er [50]. Further details will be discussed in the calculation part.

The 4886-keV level in ^{164}Gd has a very small log(ft) value for an allowed transition. This value favors 2^-, 3^-, or 4^- for its spin/parity assignment. If the spin/parity is 2^-, then it could be some other quasiparticle or collective bandhead. If the
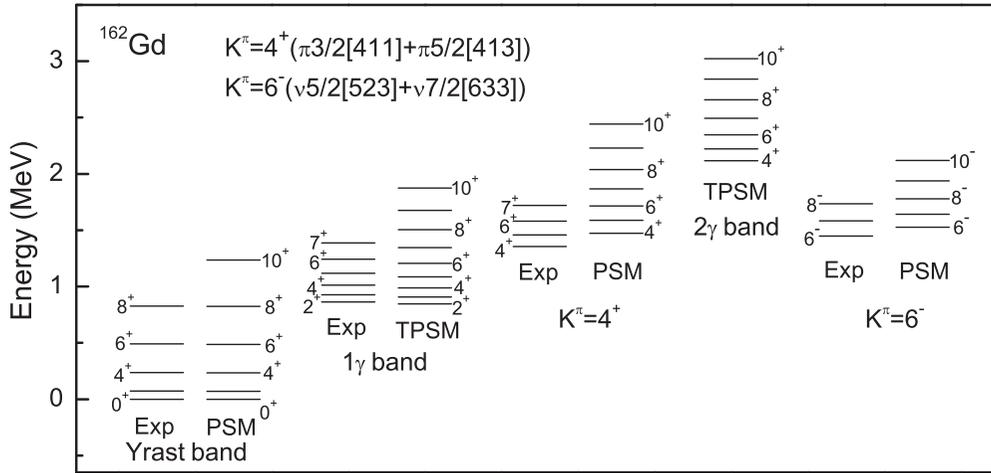
FIG. 13. Projected shell model calculations for the band structures in ^{162}Gd, compared with the experimental data.

spin/parity is 3^-, then a strong 4886-keV E3 transition would indicate strong octupole deformation or correlation. However, since the ownership of this transition is not very certain, this judgment is not very clear.

C. γ-band structure

Since the ^{160}Gd(t, p)^{162}Gd reaction [15] provided spin/parity assignments of the γ-band and β-band levels, the ^{162}Gd data obtained in the current work, together with neighboring Gd isotopes, can help investigate the γ-band structure/assignments in ^{164}Gd. From Alaga rules [49], the ratio of $B(EL)$ values for transitions out of the same state is the ratio of the square of Clebsch Gordon coefficients:

$$\frac{B(EL : J_i \to J_f)}{B(EL : J_i \to J'_f)} = \frac{\langle J_i K_i L \Delta K | J_f K_f \rangle^2}{\langle J_i K_i L \Delta K' | J'_f K'_f \rangle^2}. \quad (5)$$

This equation gives $B(E2; 2^+_\gamma \to 0^+_g)/B(E2; 2^+_\gamma \to 2^+_g) = 0.7$, $B(E2; 2^+_\gamma \to 2^+_g)/B(E2; 2^+_\gamma \to 4^+_g) = 20$,

$B(E2; 3^+_\gamma \to 2^+_g)/B(E2; 3^+_\gamma \to 4^+_g) = 2.5$, and $B(E2; 4^+_\gamma \to 2^+_g)/B(E2; 4^+_\gamma \to 4^+_g) = 0.34$. The $B(E2)$ ratios of transitions from the 966.3-keV, (2^+_γ) and 1034.7-keV, (3^+_γ) states shown in Table VI are in agreement with the Alaga rules ratio and confirm the γ-band assignment of these levels. The 4^+ level of the γ band only has one transition decaying to the 4^+ ground state. However, the Alaga rules predict the 4^+_γ to 2^+_g weaker than this 4^+_γ to 4^+_g. Detailed γ-band levels, 2γ-band levels, as well as other quasiparticle bands are discussed in the following section.

D. Projected shell model and triaxial projected shell model calculation

Projected shell model (PSM) [51–56] and Triaxial projected shell model (TPSM) calculations [57,58] have been performed for comparison with the level schemes of the g.s. bands, isomer states and γ-vibrational bands in ^{162,164}Gd. In the present calculations, the Nilsson energy levels are calculated with deformation parameters $\epsilon_2 = 0.275$, $\epsilon_4 = 0.007$,
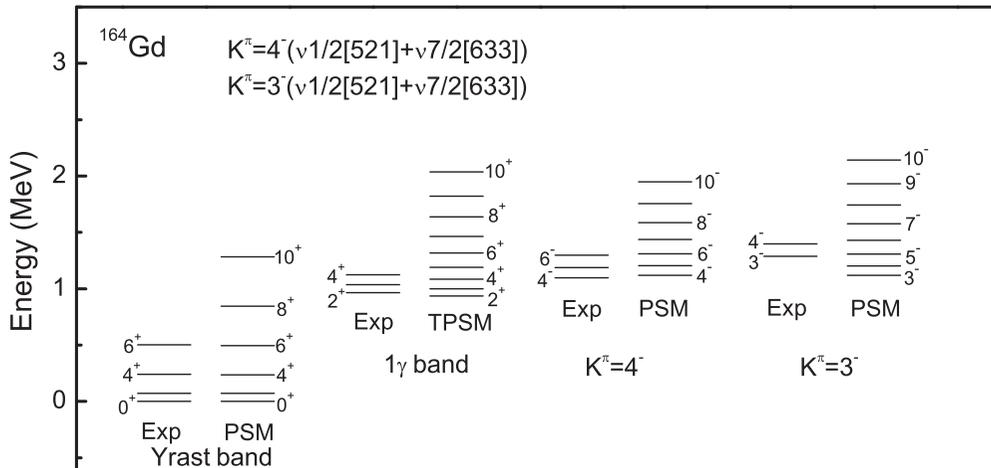
FIG. 14. Projected shell model calculations for the band structures in ^{164}Gd, compared with the experimental data.
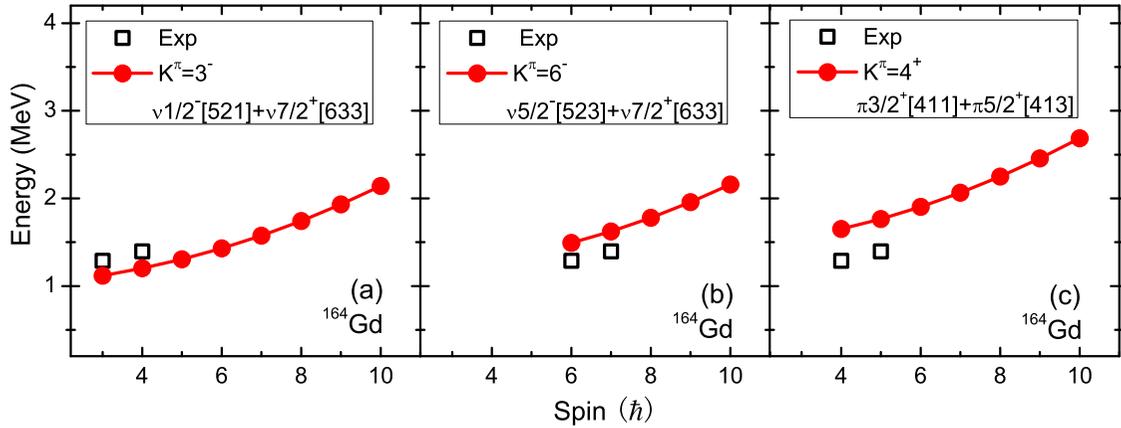
FIG. 15. The calculated energy levels of $K^\pi = 3^-$, $K^\pi = 6^-$, and $K^\pi = 4^+$ two quasiparticle bands and comparison with the experimental data.

ϵ'=0.115 for ^{162}Gd and $\epsilon_2 = 0.275$, $\epsilon_4 = 0.000$, ϵ'=0.110 for ^{164}Gd taken from Möller *et al.* [59], respectively. The ϵ' is the the triaxial deformation parameter in the TPSM calculation. The monopole-pairing strength is taken to be $G_M = [G_1 \mp G_2(N - Z)/A]/A$, "−" for neutrons and "+" for protons, with $G_1 = 20.12$ and $G_2 = 13.13$ being the coupling constants. The quadrupole-pairing strength G_Q is assumed to be proportional to G_M, with the proportionality constant being fixed to be 0.16. These strengths are consistent with those used in previous works for the same mass region [54,56].

From the calculation, the yrast band and 1γ band in ^{162,164}Gd have been well reproduced from the theory shown in Figs. 13 and 14. For ^{162}Gd, band (5) with a band-head at the 1354-keV level favors 4^+ from the decay pattern to the 1γ band (2) in Fig. 13. The calculation predicts the 2γ-band head at 2.12 MeV and the 4^+ $\pi3/2[411] \otimes \pi5/2[413]$ bandhead at 1.47 MeV. Therefore, the 4^+ band in ^{162}Gd is unlikely to be a 2γ band. Recent β-decay study [60] assigned 1071-keV 4^+ as hexadecapole band head. The 4^+ hexadecapole band in ^{160}Gd [60] has strong linking transitions to the ground state band but not the 1γ band. This decay pattern in ^{160}Gd is different from the current 4^+ band in ^{162}Gd. Thus, band (5) is proposed to be the 4^+ $\pi3/2[411] \otimes \pi5/2[413]$ two proton quasiparticle band, instead of a 2γ-vibrational band. The calculations also predict the 6^- $\nu5/2[523] \otimes \nu7/2[633]$ at 1.53 MeV giving the same assignment with Ref. [13]. Note that in Fig. 14 the 4^- $\nu1/2[521] \otimes \nu7/2[633]$ band has been very well reproduced by the PSM calculation. The configuration assignments of 6^- and 4^- isomer states in ^{162,164}Gd play an important role to discuss the location of the deformed shell gap which is discussed in Refs. [12,13,28]. Our coming theoretical work [56] will investigate the changes of deformed shell gap with the neutron numbers at $N \sim 100$ neutron-rich mass region. To discuss the configuration of the possible 3^- state with bandhead at 1289 keV in ^{164}Gd, PSM calculation is performed with the assumption of 3^-, 6^-, and 4^+ bandhead at 1289 keV and compared with the theoretical energy levels in Fig. 15. In the PSM calculation, the configurations of $K^\pi = 3^-$, $K^\pi = 6^-$, and $K^\pi = 4^+$ are assigned with $\nu1/2[521] \otimes \nu7/2[633]$,

$\nu5/2[523] \otimes \nu7/2[633]$, and $\pi3/2[411] \otimes \pi5/2[413]$. The experimental data can be well reproduced by assuming the assignment of $K^\pi = 3^-$ and $K^\pi = 6^-$, however, from the transition point of view, $K^\pi = 3^-$ $\nu1/2[521] \otimes \nu7/2[633]$ and $K^\pi = 4^+$ $\pi3/2[411] \otimes \pi5/2[413]$ configurations are reasonable to explain the observed transition of 1216 keV. For further configuration assignments of a possible 3^- state, more experimental data are expected in the future experimental work.

V. CONCLUSION

In conclusion, the structures in ^{162,164}Gd have been studied from ^{162,164}Eu β-decay. New energy levels, γ rays and band structures have been reported. The half-life of the isomeric state in ^{162}Gd has been measured for the first time. The isomeric state in ^{164}Gd has been remeasured and is in agreement with the previous measurements. Projected shell model calculations have been performed and found to be in good agreement with the experimental data for the collective and quasiparticle band structures.

[1] H. Mach, A. Piotrowski, R. L. Gill, R. F. Casten, and D. D. Warner, Phys. Rev. Lett. **56**, 1547 (1986).

[2] R. Surman, J. Engel, J. R. Bennett, and B. S. Meyer, Phys. Rev. Lett. **79**, 1809 (1997).

[3] E. F. Jones *et al.*, J. Phys. G: Nucl. Part. Phys. **30**, L43 (2004).

[4] P.-A. Soderstrom *et al.*, Phys. Rev. C **81**, 034310 (2010), and the references therein.

[5] P. Moller, J. Nix, W. Myers, and W. Swiatecki, At. Data Nucl. Data Tables **59**, 185 (1995).

[6] G. S. Simpson *et al.*, Phys. Rev. C **80**, 024304 (2009).

[7] E. Ideguchi *et al.*, Phys. Rev. C **94**, 064322 (2016).

[8] E. H. Wang *et al.*, Phys. Rev. C **90**, 067306 (2014).

[9] R. Yokoyama *et al.*, Phys. Rev. C **95**, 034313 (2017).

[10] Z. Patel *et al.*, Phys. Lett. B **753**, 182 (2016).

[11] Z. Patel *et al.*, Phys. Rev. C **96**, 034305 (2017).

[12] Z. Patel *et al.*, Phys. Rev. Lett. **113**, 262502 (2014).

[13] D. J. Hartley *et al.*, Phys. Rev. Lett. **120**, 182502 (2018).

[14] L. Gaudefroy, S. Peru, N. Arnal, J. Aupiais, J. P. Delaroche, M. Girod, and J. Libert, Phys. Rev. C **97**, 064317 (2018).

[15] G. Lovhoiden *et al.*, Phys. Scr. **34**, 691 (1986).

[16] A. Osa, S. ichi Ichikawa, M. Matsuda, T. K. Sato, and S.-C. Jeong, Nucl. Instrum. Methods Phys. Res., Sect. B **266**, 4394 (2008).

[17] R. C. Greenwood, R. A. Anderl, J. D. Cole, and H. Willmes, Phys. Rev. C **35**, 1965(R) (1987).

[18] J. C. Chang, G. Schupp, and R. R. Hurst, Nucl. Phys. A **142**, 634 (1970).

[19] R. J. Gehrke, R. C. Greenwood, J. D. Baker, and D. H. Meikrantz, Radiochim. Acta **31**, 1 (1982).

[20] R. C. Greenwood, M. A. Lee, and R. A. Anderl, Radiochim. Acta **43**, 129 (1988).

[21] J. A. Winger *et al.*, Phys. Rev. C **81**, 044303 (2010).

[22] M. F. Alshudifat *et al.*, Phys. Rev. C **93**, 044325 (2016).

[23] M. Asai *et al.*, in *Proceedings of the 3rd International Conference on Fission and Properties of Neutron-rich Nuclei*, edited by J. H. Hamilton, A. V. Ramayya, and H. K. Carter (World Scientific, Singapore, 2002), p. 227.

[24] D. Rabenstein and H. Vonach, Z. Naturforsch. **26a**, 458 (1971).

[25] B. Singh, Nucl. Data Sheets **105**, 223 (2005).

[26] R. Orford, F. G. Kondev, G. Savard, J. A. Clark, W. S. Porter, D. Ray, F. Buchinger, M. T. Burkey, D. A. Gorelov, D. J. Hartley, J. W. Klimes, K. S. Sharma, A. A. Valverde, and X. L. Yan, Phys. Rev. C **102**, 011303(R) (2020).

[27] M. Vilen *et al.*, Phys. Rev. C **101**, 034312 (2020).

[28] J. Wu *et al.*, Phys. Rev. Lett. **118**, 072701 (2017).

[29] S. Ichikawa, M. Asai, K. Tsukada, H. Haba, Y. Nagame, M. Shibata, M. Sakama, and Y. Kojima, Phys. Rev. C **71**, 067302 (2005).

[30] A. Etile *et al.*, Phys. Rev. C **91**, 064317 (2015).

[31] P. Hoff and B. Fogelberg, Nucl. Phys. A **368**, 210 (1981).

[32] K. Miernik *et al.*, Phys. Rev. C **90**, 034311 (2014).

[33] X. Y. Wu, S. K. Ghorui, L. J. Wang, Y. Sun, M. Guidry, and P. M. Walker, Phys. Rev. C **82**, 064314 (2010).

[34] C. M. Baglin, Nucl. Data Sheets **109**, 2257 (2008).

[35] J. K. Tuli and E. Browne, Nucl. Data Sheets **157**, 260 (2019).

[36] L.-C. He *et al.*, Chin. Phys. C **41**, 044003 (2017).

[37] J. Katakura and K. Kitao, Nucl. Data Sheets **97**, 765 (2002).

[38] D. Nagae *et al.*, AIP Conf. Proc. **1224**, 156 (2010).

[39] B. Singh and J. Chen, Nucl. Data Sheets **147**, 1 (2018).

[40] T. Kibedi *et al.*, Nucl. Instrum. Methods Phys. Res., Sect. A **589**, 202 (2008).

[41] R. A. Anderl and R. C. Greenwood, J. Radioanal. Nucl. Chem. **142**, 203 (1990).

[42] C. W. Reich, Nucl. Data Sheets **112**, 2497 (2011).

[43] C. J. Zachary *et al.*, Phys. Rev. C **101**, 054312 (2020).

[44] A. K. Jain, A. Ghosh, and B. Singh, Nucl. Data Sheets **107**, 1075 (2006).

[45] C. W. Reich, Nucl. Data Sheets **113**, 157 (2012).

[46] H. Hayashi *et al.*, Nucl. Instrum. Methods A. **747**, 41 (2014).

[47] M. Wang, G. Audi, F. G. Kondev, W. J. Huang, S. Naimi, and X. Xu, Chinese Phys. C **41**, 030003 (2017).

[48] S. R. Lesher *et al.*, Phys. Rev. C **95**, 064309 (2017).

[49] G. Alaga, Phys. Rev. **100**, 432 (1955).

[50] C. Y. Wu, D. Cline, M. W. Simon, R. Teng, K. Vetter, M. P. Carpenter, R. V. F. Janssens, and I. Wiedenhover, Phys. Rev. C **68**, 044305 (2003).

[51] K. Hara and Y. Sun, Int. J. Mod. Phys. E **4**, 637 (1995).

[52] Y. Sun, Phys. Scr. **91**, 043005 (2016).

[53] Y. X. Liu, Y. Sun, X. H. Zhou *et al.*, Nucl. Phys. A **858**, 11 (2011).

[54] Y. C. Yang, Y. Sun, S. J. Zhu *et al.*, J. Phys. G: Nucl. Part. Phys. **37**, 085110 (2010).

[55] X. Y. Wu, S. K. Ghorui, L. J. Wang, Y. Sun, M. Guidry, and P. M. Walker, Phys. Rev. C **95**, 064314 (2017).

[56] Y. X. Liu, C. J. Lv, Y. Sun, and F. G. Kondev, J. Phys. G: Nucl. Part. Phys. **47**, 055108 (2020).

[57] J. A. Sheikh and K. Hara, Phys. Rev. Lett. **82**, 3968 (1999).

[58] Y. Sun, K. Hara, J. A. Sheikh, J. G. Hirsch, V. Velazquez, and M. Guidry, Phys. Rev. C **61**, 064323 (2000).

[59] P. Möller, A. Sierk, T. Ichikawa *et al.*, At. Data Nucl. Data Tables **109-110**, 1 (2016).

[60] D. J. Hartley *et al.*, Phys. Rev. C **101**, 044301 (2020).